Characterisation of cell cycle checkpoint kinases in *Toxoplasma gondii*

Monique K. Johnson[1], Sara Chelaghma[2], Ludek Koreny[2], Ross F. Waller[2], Catherine J. Merrick[1*]

[1] Department of Pathology, University of Cambridge, Tennis Court Road, Cambridge, CB2 1QP, UK.

[2] Department of Biochemistry, University of Cambridge, Tennis Court Road, Cambridge, CB2 1QW, UK.

* To whom correspondence should be addressed:

Department of Pathology, Cambridge University, Tennis Court Road, Cambridge, CB2 1QP, UK

Tel: (+44) 1223 333330

Email: cjm48@cam.ac.uk

ABSTRACT

Toxoplasma gondii is a protozoan parasite in the apicomplexan phylum. Apicomplexan parasites replicate using a variety of non-canonical cell division modes, distinct from binary fission, whose molecular regulation is incompletely understood. *T. gondii* replicates by endodyogeny in its intermediate hosts, and by schizogony in its definitive host. To improve our understanding of how these unusual, flexible cell division modes are regulated, we characterised the *T. gondii* homologues of the cell-cycle checkpoint kinases ATM and ATR. These phosphoinositol-3-kinase-like kinases are entirely absent in some related parasites including *Plasmodium*; in *T. gondii* they are present but their putative checkpoint roles were uncharacterised. Both *Tg*ATM and *Tg*ATR were found to be dispersed throughout the parasite and they did not detectably relocate to the nucleus after DNA damage. Nevertheless, they were both required for checkpoint responses to DNA damage, including acute replication slowing and phosphorylation of the DNA damage marker histone H2AX. Unusually, the two kinases seemed to cooperate in the checkpoint response, with the loss of either one largely ablating the response, regardless of the type of DNA damage. Thus, *T. gondii* clearly retains a DNA-damage-responsive checkpoint, but some of its key features differ from the well-studied checkpoint in human cells.

KEYWORDS

Toxoplasma, cell cycle, checkpoint, PIKK, ATM, ATR

INTRODUCTION

The apicomplexan parasite *Toxoplasma gondii* is a significant cause of disease in both animals and humans. It is widespread in the global human population as a largely asymptomatic infection, but it can cause severe birth defects if pregnant women are acutely infected, potentially lethal disease in immunocompromised patients, and retinal scarring and blindness in immunocompetent individuals. Accordingly, effective drugs are required to treat acute toxoplasmosis, and concerns have recently been raised about resistance to current therapies (Montazeri, Mehrzadi et al. 2018). These therapies usually consist of anti-folate regimes such as pyrimethamine/sulfadiazine (Neville, Zach et

al. 2015), which act to suppress folate metabolism, starve the parasite of nucleotide precursors and suppress its replication. A detailed understanding of the parasite's mode of replication is therefore important – both to understand the action of anti-parasite drugs, and also because *Toxoplasma* replication is fundamentally unusual. As such, it can illuminate our understanding of the basic biology of eukaryotic cell division.

Toxoplasma lies in the apicomplexan phylum of protozoan parasites and a key feature of this deeply-diverging phylum is that the species therein do not replicate by conventional binary fission – the cell division mode used by most model cells from *S. cerevisiae* to human. Instead, they employ a variety of syncytial division modes, such as endodyogeny in *Toxoplasma*, endopolygeny in *Sarcocystis* and schizogony in the malaria parasite *Plasmodium* (Striepen, Jordan et al. 2007, Francia and Striepen 2014). Many of the regulatory proteins that drive and control the *Toxoplasma* cell cycle are now being identified (Suvorova, Francia et al. 2015, Alvarez and Suvorova 2017, Sinai and Suvorova 2020, Gubbels, Coppens et al. 2021, Hawkins, Naumov et al. 2021) but comparatively little is known about stress-responsive checkpoints within this cycle.

Eukaryotic cells make highly conserved 'checkpoint' responses to DNA damage or stalled replication, involving a kinase cascade that arrests the cell cycle and promotes DNA repair (Zhou and Elledge 2000). This is initiated by one or more members of the phosphoinositol-3-kinase-like kinase (PIKK) family. These kinases – Mec1 in budding yeast; ATM and ATR in humans – have a catalytic domain that is structurally related to PI3K lipid kinases (Perry and Kleckner 2003) but they act upon protein substrates instead, including the checkpoint-transducing kinases Rad53/Chk1/Chk2 and the histone H2AX, which marks damaged DNA for repair.

As an obligate intracellular parasite, *Toxoplasma* can certainly suffer DNA damage through inflammatory stress, oxidative and free-radical damage, etc. Like most eukaryotes, it encodes pathways to repair DNA double-strand breaks (DSBs), i.e. homologous recombination and non-homologous end-joining (Fenoy, Bogado et al. 2016). Therefore, it would make evolutionary sense to retain DNA-damage-responsive checkpoints. Curiously, these may be absent in at least some apicomplexans: *Plasmodium* species seem to entirely lack PIKK kinases (Matthews, Duffy et al. 2018), and may not arrest their cycle after aberrant genome replication (Absalon and Dvorin 2021, Matthews, McDonald et al. 2022). *Toxoplasma*, by contrast, does encode PIKK homologues, but their DNA damage checkpoint has not been thoroughly investigated, despite its potential importance as a target for anti-parasite drugs (Angel, Vanagas et al. 2020).

Here, we characterised for the first time the two PIKKs in *T. gondii*, which are annotated *Tg*ATM and *Tg*ATR, according to their homology with human ATM and ATR. Both genes were categorised as 'fitness conferring' in a Crispr-based gene knockout screen (Sidik, Huet et al. 2016). To our knowledge, *Tg*ATR was entirely unstudied, while *Tg*ATM was first identified in 2010 (Vonlaufen, Naguleswaran et al. 2010) in a study of the acetyltransferase *Tg*MYST. This found that *Tg*MYST may induce a putative ATM homologue, and also inferred that *Tg*ATM may phosphorylate *Tg*H2AX. A slow-growth phenotype when *Tg*MYST was over-expressed was taken to represent *Tg*ATM-induced checkpoint activity, and was ablated by an inhibitor of human ATM, KU-55933. A subsequent study also used this inhibitor and showed that KU-55933 itself could slow *T. gondii* growth, and abolish H2AX phosphorylation after DNA damage (Munera Lopez, Ganuza et al. 2019).

Hence, there was circumstantial evidence that *Tg*ATM acts as DNA damage checkpoint kinase, and could be essential for replication by endodyogeny. Here, we report that *Tg*ATM and *Tg*ATR can both be knocked down without any fitness defect in cultured parasites, but that both proteins – in a largely overlapping manner – do enforce a DNA damage checkpoint in *T. gondii.*

RESULTS

T. gondii encodes homologues of cell cycle checkpoint kinases

Figure 1 shows the results of a phylogenetic analysis of *T. gondii* PIKK homologues. We identified single homologues of ATM, ATR, DNA-PK and TOR, each of which was most closely related to the respective human homologue. The nearest *T. gondii* homologue of DNA-PK was annotated in ToxoDB only as a PI3/4 kinase, whereas the *T. gondii* homologues of ATM, ATR and TOR were annotated as putative forms of these three proteins. *T. gondii* also encoded single homologues of the lipid kinases PI3K and PI4K, branching separately from all PIKKs. They were, again, annotated in ToxoDB only as 'PI3/4 kinases' but one gene clearly grouped with PI3Ks, and the other gene with PI4Ks, from both human and *Plasmodium* species.

In the PIKK family, ATM in human cells responds primarily to DNA DSBs, while ATR responds primarily to stalled replication forks (Helt, Cliby et al. 2005). DNA-PK is involved in executing non-homologous end joining and TOR has a different cell-cycle role, regulating cell growth and protein production. Therefore, in *T. gondii*, homology would suggest that '*Tg*ATM' and '*Tg*ATR' should be most directly involved in DNA-damage checkpoint responses to DNA DSBs and stalled replication forks respectively. However, neither protein had yet been investigated, localised in the parasite cell, characterised for kinase activity, or knocked out to determine essentiality.

Inducible knockdown of *Tg*ATM and *Tg*ATR

PIKKs are very large proteins: *Tg*ATM has a predicted size of ~250kDa, and *Tg*ATR, ~650kDa. Cloning for overexpression or recombinant expression would be prohibitively difficult, as would biochemical purification of these proteins. We therefore addressed the function of *Tg*ATM and *Tg*ATR by making inducible knockdowns, since a genome-wide screen for essential genes in *T. gondii* had previously suggested that both genes may be refractory to complete knockout (Sidik, Huet et al. 2016) (Figure S1A, B).

The strategy for gene tagging and inducible knockdown is shown in Figure 2A and B: 5' integration of a haemagglutinin (3xHA) tag and a tetracycline-repressible promoter (Meissner, Brecht et al. 2001, Barylyuk, Koreny et al. 2020). PCR genotyping of the resultant mutants confirmed correct integration (Figure S1C, D). Upon induction of knockdown with anhydrotetracycline (ATc), western blotting showed that all detectable HA-tagged *Tg*ATM was lost within 24h and this depletion was stable through 72h (Figure S1E). A similar assessment of the *Tg*ATR knockdown was not possible because the protein was too large for effective western blotting. However, immunofluorescence assays (IFA) showed the near-total loss of both proteins within 24h (Figure 2C, D) and this was confirmed by quantifying the immunofluorescent signals. Residual fluorescence after knockdown was similar to the levels seen in parental cells without any HA-tagged protein (Figure 2E, F).

Human ATM and ATR have a primarily nuclear location, consistent with their function (Keegan, Holtzman et al. 1996). Interestingly, however, the reporter-tagged forms of both *Tg*ATM and *Tg*ATR were detected throughout the cell (Figure 2C, D), and their diffuse appearance was

inconsistent with localisation to any subcellular organelle. It is notable that *Tg*MYST, which has been proposed to acetylate *Tg*ATM, was also reported to be cytoplasmic, contrary to its expected nuclear location (Vonlaufen, Naguleswaran et al. 2010). Neither *Tg*ATM nor *Tg*ATR appeared in the published subcellular atlas of the *Toxoplasma* proteome (Barylyuk, Koreny et al. 2020), and the difficulty of handling such large, unstable proteins precluded subcellular fractionation for western blotting to conclusively determine the proportions of *Tg*ATM and *Tg*ATR in nuclear and cytoplasmic fractions.

Knockdown of *Tg*ATM or *Tg*ATR imposes no growth defect or DNA-damage-sensitivity in culture

Contrary to predictions from the genome-wide screen (Sidik, Huet et al. 2016), neither gene knockdown showed an overt growth phenotype in triplicate plaque assays (Figure 3A, B). We therefore concluded that *Tg*ATM and *Tg*ATR were either entirely dispensable for parasite growth in normal culture conditions, or that these proteins were essential but that residual protein after knockdown, albeit undetectable on western blots, could suffice under normal conditions. In either case, challenging the parasites with DNA damage might reveal an effect on parasite growth. Therefore, parasites were subjected to two DNA damaging agents, the alkylating agent methyl methane sulphonate (MMS) or the topoisomerase inhibitor camptothecin (CPT) (previously validated to cause H2AX phosphorylation in this system (Munera Lopez, Ganuza et al. 2019)).

Both agents caused a titratable defect in parasite growth, the nature of which appeared to be different for MMS versus CPT. MMS primarily reduced the number of plaques, suggesting acute parasite killing followed by rapid decay of alkylating activity, so that surviving parasites grew quite normally over the subsequent 10 days. CPT reduced both the number and size of plaques that grew after 10 days, suggesting ongoing growth-inhibitory activity as well. However, none of these effects was clearly exacerbated by the knockdown of either PIKK (Figure 3C, D).

Knockdown of *Tg*ATM or *Tg*ATR ablates acute checkpoint-like responses to DNA damage

We then reasoned that long-term growth assays might not be a suitable read-out if the knockdowns did, in fact, impede a DNA damage checkpoint. Parasites that failed to respond to DNA damage and continued to replicate, rather than inducing DNA repair, might initially have a growth advantage but might eventually die if their genome was irreparably damaged. Hence the outcome of a 10-day plaque assay might appear similar whether a checkpoint was induced or not. Accordingly, we sought more acute phenotypes in the knockdown parasites.

A 24h 'replication assay' can quantify parasite growth during just the first ~3 cycles of endodyogeny after invasion, by counting the numbers of parasites in newly formed vacuoles in individual host cells (Figure 4A). This assay confirmed that replication rates were indeed normal in both knockdown lines. DNA damage induced by either MMS or CPT could reduce the initial replication rate and the knockdown of either PIKK ablated this (Figure 4B, C), implying that cell-cycle slowing after DNA damage was indeed the result of checkpoint induction, and that knockdown parasites failed to induce such a checkpoint. There was little difference between the *Tg*ATM and *Tg*ATR knockdowns, suggesting substantial cooperation between the two proteins, with both being similarly required for an effective checkpoint response to two types of DNA damage: alkylation or topoisomerase inhibition. Of note, the *Tg*ATM knockdown only partially restored replication to normal rates after CPT damage, but did fully restore it after MMS damage at 25μM, and almost fully after 50μM. The *Tg*ATR knockdown only partially restored replication to normal rates after MMS damage, but did fully restore it after CPT damage. This suggests that there is some degree of

specialisation between the two proteins according to different types of DNA damage, but both proteins were clearly required for a fully effective response.

We then measured a second acute read-out for the DNA damage checkpoint: phosphorylation of histone H2AX. This appeared at substantial levels in normally replicating parasites, as previously reported (Dalmasso, Onyango et al. 2009, Nardelli, Che et al. 2013, Bogado, Dalmasso et al. 2014), suggesting a high endogenous level of replication stress in cultured tachyzoites. Phosphorylation appeared to be induced even further by DNA damage, particularly via CPT, with brighter and larger foci of phosphorylated H2AX appearing (Figure 4D, E). Either knockdown ablated the γH2AX signal almost entirely, and it could not be induced even after DNA damage. Again, both proteins were apparently required, since either individual knockdown affected H2AX phosphorylation equally severely.

<u>*Tg*ATR does not behave quantifiably differently in the presence or absence of *Tg*ATM</u>

We wished to investigate the extent and nature of cooperation between *Tg*ATM and *Tg*ATR. Accordingly, we added a second, distinguishable tag (3x V5) to the ATR gene in the HA-tagged, inducible knockdown line for *Tg*ATM (Figure 5A, Figure S2). Thus, we could follow the location and quantity of *Tg*ATR in cells with *Tg*ATM either present or absent.

Figure 5B shows that there was no substantial colocalisation of the two proteins: both appeared in speckles throughout the parasite that were largely non-overlapping. There was also no clear difference, detectable by immunofluorescence, in the location or amount of *Tg*ATR in the presence or absence of *Tg*ATM. The assessment of representative immunofluorescence images is inherently qualitative, so we also quantified the signals in cohorts of cells: both the amount of signal across individual parasites, and the maximum brightness of foci per parasite. There was considerable variation in both parameters, but ATR foci did not become reproducible fainter, brighter or more abundant in the absence of *Tg*ATM (Figure 5C, D). Therefore, although the two proteins were required in concert to induce checkpoint phenotypes (Figure 4), we could not detect any direct interaction between them. Finally, we checked whether the distribution of either protein changed after DNA damage, specifically to concentrate in the nucleus, as might be expected if a DNA damage response was required there. When the proportion of signal in the nucleus versus cytoplasm was quantified in cohorts of cells before or after DNA damage, no clear differences were seen (Figure S3).

<u>A specific inhibitor of human ATM does not phenocopy the knockdown of *Tg*ATM or *Tg*ATR</u>

Previous publications used the human ATM inhibitor KU-55933 on the assumption that it would be equally specific for *Tg*ATM (Vonlaufen, Naguleswaran et al. 2010, Munera Lopez, Ganuza et al. 2019). We tested this by comparing the effect of KU-55933 with the effect of knocking down *Tg*ATM. Figure 6A shows that the KU-55933 inhibitor caused a dose-dependent growth defect in a 10-day plaque assay, in contrast with either individual knockdown, which did not (Figure 3). Furthermore, the growth defect imposed by the inhibitor was similar whether an individual PIKK was also knocked down or not (Figure 6B). This led to two potential conclusions: either the effect of KU-55933 was 'off target' (via a pathway unrelated to *Tg*ATM/*Tg*ATR), or alternatively, the inhibitor was targeting both PIKKs and this complete loss of function was more deleterious for *T. gondii* than the loss of either one alone.

We checked whether treatment with KU-55933 could affect either the amount of *Tg*ATM or *Tg*ATR in individual parasites, or the maximum brightness of their foci per parasite, by quantifying

IFA images as in figure 5. No consistent changes were detected in the foci of either protein (except, as expected, when *Tg*ATM was knocked down) (Figure 6C). However, when the total quantity of protein per parasite was measured, KU-55933 treatment did correlate with an overall increase in the amount of *Tg*ATM, whereas there was no change in *Tg*ATR (Figure 6D). This implied that KU-55933 might indeed inhibit *Tg*ATM and that the parasite might respond to this by upregulating *Tg*ATM expression.

To further distinguish between the possibilities of off-target killing or pan-PIKK inhibition, we checked the previously published result that cells treated with KU-55933 could not phosphorylate H2AX (Munera Lopez, Ganuza et al. 2019). This was confirmed: the inhibitor largely prevented γH2AX foci from forming, both in endogenous replication and in response to DNA damage (Figure 6E), and H2AX phosphorylation was equally inhibited in the human host cell nuclei, as expected (Figure S4). In this regard, inhibitor-treatment was similar to the individual knockdown of *Tg*ATM (or *Tg*ATR). Therefore, it appeared likely that KU-55933 did in fact inhibit *Tg*ATM, but that it additionally affected *Tg*ATR and/or other off-target proteins, resulting in a growth defect.

DISCUSSION

This work characterised the two PIKK homologues in *Toxoplasma gondii*, with the aim of establishing whether or not they act as DNA damage checkpoint kinases. This was an important question because toxoplasmosis is often treated with drugs that may cause DNA damage, and also because it could help to establish how damage-responsive checkpoints have evolved across the apicomplexan phylum. In this large phylum of early-diverging protists, some parasites, like *T. gondii*, retain PIKK homologues while other important parasites, like *Plasmodium* spp., appear to have lost them.

We established, phylogenetically, that *T. gondii* does encode orthologues of all the classes of PIKKs defined in human cells. We then tagged and knocked down the orthologues of ATM and ATR. The first striking observation was that neither protein was primarily nuclear, but appeared diffusely throughout the cytoplasm, in largely non-overlapping speckles that were inconsistent with any particular organelle. It is notable that another protein with a predicted nuclear role, the acetyltransferase *Tg*MYST, was also reported thus (Vonlaufen, Naguleswaran et al. 2010), and proposed to shuttle to the nucleus. In human cells, although ATM is nuclear, it can under some stimuli shuttle to the cytoplasm (Wu, Shi et al. 2006). We, however, found no clear evidence that either *Tg*ATM or *Tg*ATR shuttled between cytoplasm and nucleus after DNA damage.

Both *Tg*ATM and *Tg*ATR were then inducibly knocked down, with near-100% efficiency as seen by immunofluorescence (and also by western blotting in the case of *Tg*ATM). As with any inducible gene regulation, some residual protein might remain. However, under severe-knockdown conditions, we found no evidence that either protein was essential or had any effect on normal cell growth. Nevertheless, after DNA damage, both knockdowns did ablate an acute reduction in cellular replication, as well as another key marker of the DNA damage response: phosphorylation of histone H2AX. Thus, there was strong evidence for a canonical checkpoint role for *Tg*ATM and *Tg*ATR. This was not initially detected in plaque assays simply because parasites that failed to respond to DNA damage and continued to replicate would probably die from irreparable genome damage before a large plaque could be formed.

In human cells, ATR responds primarily to stalled replication forks and ATM, to DNA DSBs (Falck, Petrini et al. 2002). To establish whether *Tg*ATM and *Tg*ATR acted similarly, we used two different DNA damaging agents, the alkylating agent MMS, well-established to cause fork stalling at

alkylated bases, and the topoisomerase inhibitor CPT, which can induce DNA breaks. (Of note, our knockdowns were made in a background deficient for non-homologous end-joining, but still competent to repair DSBs by homologous recombination.) Interestingly, we detected little 'division of labour' between *Tg*ATM and *Tg*ATR: the phenotypes in H2AX phosphorylation and cellular replication were similarly affected by both knockdowns. The only detectable difference was that high concentrations of MMS still elicited some replication-slowing when *Tg*ATR was lost, but not when *Tg*ATM was lost, and the converse was true of CPT, suggesting that *Tg*ATM may be more important in responding to alkylation damage and *Tg*ATR, to DNA breakage. This would be the opposite specialisation of protein function to that in human cells. Generally, however, both proteins were required to induce both types of DNA-damage checkpoint.

Despite this, we found no evidence for their colocalization or reciprocal up/down-regulation, so it is unlikely that the two proteins act in a complex (stringent biochemical assays with these exceptionally large proteins would be required to establish this conclusively). Mutual regulation, such as transphosphorylation, may be more likely. In human cells, ATM exists as an inactive dimer and is induced to autophosphorylate after DNA damage, whereupon it dissociates and its monomers act on downstream substrates (Bakkenist and Kastan 2003). Perhaps in *T. gondii*, activating phosphorylation event(s) occur in trans and require both PIKKs. Alternatively, both PIKKs might act in mutually-essential ways on a single transducing protein downstream (whereas in humans, ATM and ATR activate Chk2 and Chk1 respectively (Falck, Petrini et al. 2002)).

We attempted to further separate the activities of the two proteins using a 'specific' small-molecule inhibitor of human ATM, KU-55933, but this did not phenocopy the *Tg*ATM knockdown. The inhibitor severely affected cell growth, suggesting either off-target effects or an equal inhibition of both PIKKs, with this being more deleterious than either single knockdown. Since the inhibitor ablated H2AX phosphorylation, and had the same effect with or without either genetic knockdown, we favoured the latter explanation. Although we were unable to generate a double genetic knockdown, KU-55933 may itself generate this effect. If so, this implies that the complete loss of all PIKK activity does affect cell growth and viability – as expected, since DNA damage occurs during normal replication (as marked by γH2AX), and constant checkpoint activation is probably required in replicating tachyzoites. Curiously, *Tg*ATM and *Tg*ATR seem to be mutually required for this, but perhaps in each genetic knockdown, a low residual level of either protein could transphosphorylate the other, yielding a low-level response and cell survival, whereas KU-55933-treated cells could make no response at all.

Overall, we conclude that *T. gondii* does have PIKK kinases that enforce a DNA-damage checkpoint, slowing down cellular replication and phosphorylating the DNA damage marker H2AX. Unusually, both *Tg*ATM and *Tg*ATR seem to be equally required for this, regardless of the type of DNA damage. This could possibly represent a step towards reductive evolution to a single PIKK, since these proteins are variably represented in apicomplexan parasites. For example, *T. gondii* and close relatives such as *Cystoisospora suis* have homologs of both ATM and ATR; *Eimeria acervulina* appears to have only an 'ATM'; *Babesia microti* and *Theileria parva*, only an 'ATR', and *Cryptosporidium hominis*, two closely-related ATR-like proteins (Figure S5). Such variation might, in turn, help to explain the situation in *Plasmodium*, where PIKK homologues are entirely lost (Figure 1, S5). (Whether checkpoint activity is then lost in *Plasmodium*, or transferred to another protein, remains to be explored.)

In terms of cell division, apicomplexan parasites are particularly interesting because they can divide by different modes at different lifecycle stages. For example, *Plasmodium* uses schizogony in the blood stage and something resembling endopolygeny in the oocyst (Araki, Kawai et al. 2020); *T. gondii* uses endodyogeny in intermediate hosts and schizogony – apparently analogous to the schizogony in *Plasmodium* – in the definitive feline host (Hutchison, Dunachie et al. 1970, Gubbels, Keroack et al. 2020). Whether DNA damage checkpoints are equally active in both stages cannot presently be investigated, because experimental access to the schizogony stage in *T. gondii* is very limited. Nevertheless, further investigation of cell-cycle checkpoints in *T. gondii* might usefully inform the study of checkpoints in other apicomplexans such as *Plasmodium* as well.

MATERIALS AND METHODS

Phylogenetics

MUSCLE alignment of amino acid sequences was completed in UGENE (v49.1). ClustalW output of MUSCLE alignment was used to make the tree in IQtree (v.1.6.12) (Trifinopoulos, Nguyen et al. 2016), which calculated a best fit model (Kalyaanamoorthy, Minh et al. 2017). VT+F+R3 was the Model chosen. The tree was rooted with human and yeast outgroup in Figtree (v1.4.4). Bootstrap node support values were calculated as percentages of 1000 'run tree' iterations.

Parasite strains and growth

T. gondii tachyzoites from the strain RH and derived strains, including Δ*ku80*:TATi tachyzoites (a gift from Lilach Sheiner and Boris Striepen, University of Georgia) (Sheiner, Demerly et al. 2011), were grown on a confluent monolayer of human foreskin fibroblast (HFF) cells in 10 ml flasks of ED1 (Dulbecco's Modified Eagles Medium supplemented with 1% foetal bovine serum (FBS), 0.2 mM L-glutamine, 0.25 µg ml^{-1} Fungizone (ThermoFisher), 10 unit ml^{-1} penicillin and 10 µg ml^{-1} streptomycin (ThermoFisher)) and maintained at 37 °C with 10% CO_2, as previously described (Roos, Donald et al. 1994).

Creation of transgenic *T. gondii*

Gene tagging was performed as described by Waller and colleagues (Barylyuk, Koreny et al. 2020). A CRISPR/Cas9-assisted, PCR-mediated tagging strategy was used to perform endogenous gene tagging with epitope tags and/or endogenous promoter replacement with an ATc-regulatable t7s4 promoter. The generation of transgenic *T. gondii* involved a level M Cas9/sgRNA plasmid, P5, containing a specific protospacer sequence for directing a locus-specific DNA break to facilitate homologous recombination-driven insertion of the donor DNA fragment. Protospacer sequences were designed for insertion into the N-terminus of genes encoding putative *T. gondii* homologues of ATR (TGGT1_283702) and ATM (TGGT1_248530) (Figure S6B). The donor DNA fragment was PCR amplified from one of the template plasmid vectors (Figure S6A) using primers (Figure S6B) that included specific homology arms directing the integration of this donor DNA construct into the target genetic locus for ATM and ATR. Electroporation of these constructs was completed as in (Barylyuk, Koreny et al. 2020).

Parasite genomic DNA extraction for PCR confirmation

T25 flasks containing mostly extracellular *T. gondii* were scraped and host cell debris was pelleted at 100 *xg* for 5 min. A 1-1.5 ml aliquot was harvested from the supernatant, containing 0.5-5 x 10^6 fully

lysed *T. gondii* tachyzoites, and these were collected by centrifugation (7,000 *xg*/full speed, 2 min). The cell pellet was resuspended in 20 µl proteinase K solution: 5% proteinase K (Thermo Scientific, EO0491), 10% PCR buffer 10x (Roche, 11732650001), 85% dH_2O. This was incubated at 45 °C for 60 min. The proteinase was heat inactivated at 94 °C for 10 min. The remaining solution was used to run PCR directly, 0.3 - 1.5 µl as DNA template for a 20 µl PCR reaction.

Plaque assay

Plaque assays required parasites derived from freshly lysed host cells, which were centrifuged at 100 *xg* for 5 min to remove host cell debris. The same number of parasites (around 500) was added to each new T25 flask containing HFF monolayer. In experiments testing the knockdown (k/d) of a target gene, a control of untreated *T. gondii*-infected HFFs was used, as well as ATc-treated (k/d) *T. gondii*-infected HFFs. For the ATc treatment, 0.5 µg/ml of ATc was added. After 10 days of incubation at 37 °C and with 10% CO_2, the media from flasks was aspirated and the cells were washed once with PBS. Cells were fixed with 5 ml of 100% ice-cold methanol for 5 min and stained with 5 ml of 1% crystal violet solution for 15 min. After staining, crystal violet solution was removed and flasks were washed three times with PBS. Flasks were allowed to dry, then imaged for qualitative analysis.

Immunofluorescence

T.gondii infected HFFs were grown on glass coverslips in 6 well plates. Cells were fixed to coverslips with 2% PFA/PBS for 15 min at RT and permeabilised with 0.02% TritonX100 in PBS for 10 min. Cells were blocked for 1 h in 2% BSA/PBS. Coverslips were incubated with primary antibody in blocking solution for 1 h and then incubated in secondary antibodies in 2% BSA/PBS for 1 h in the dark. 120 µl of 2 µg/ml DAPI solution (Merck) was added for 10 min and then coverslips were mounted on slides in ProLong® Diamond Antifade (ThermoFisher, P36961). Images were acquired using a Nikon Eclipse Ti widefield microscope with a Nikon objective lens (Plan APO, 100x/1.45 oil), and a Hamamatsu C11440, ORCA Flash 4.0 camera. Images were processed using the NIS-Elements software and ImageJ (v.1.51w).

Replication assay

For the replication assay parasites were pre-treated with or without ATc for 48 h. Parasites derived from freshly lysed host cells were counted and an equal number (1.6×10^6) was added to HFF monolayers grown on coverslips in 6-well plates. Cells were incubated for 2 h at 37 °C to allow invasion. Parasites that had not invaded were washed off three times with warm ED1. Parasites were then allowed to grow for a further 24 h with or without ATc, then fixed as per the protocol for immunofluorescence and mounted onto slides using DAPI stain only. Images were acquired using a Nikon Eclipse Ti widefield microscope with a Nikon objective lens (Plan APO, 100x/1.45 oil), and a Hamamatsu C11440, ORCA Flash 4.0 camera. Images were processed using the NIS-Elements software and ImageJ (v.1.51w). Numbers of parasites in each vacuole were counted for 250 vacuoles per condition.

Immunoblotting

Approximately 50×10^6 parasites were purified from the host cell debris by filtration through 3-µm-pore-size polycarbonate film membrane filters (Nuclepore Track-Etch Membrane, Whatman). Cells were collected and washed in PBS by centrifugation at 1,700 × *g* for 10 min at RT, then pellets were resuspended in 1x RIPA buffer (150 mM sodium chloride, 1.0% NP-40 or Triton X-100, 0.5% sodium

deoxycholate, 0.1% SDS (sodium dodecyl sulfate) and 50 mM Tris pH 8, added to 50 ml dH_20). Protease inhibitors (ROCHE, cOmplete Mini) were added to 10 ml aliquots directly before use). Samples were freeze-thawed 3 times by placing tubes in dry ice / 100% ethanol and a heated Eppendorf block at 37 °C. Cell debris was pelleted at 4 °C at 13,000 *xg*, then supernatant was removed to a new Eppendorf. 1 x NuPage LDS Sample Buffer (ThermoFisher: NP0007), supplemented with 0.1% 2-mercaptoethanol, was added to samples and boiled at 90 °C for 5 min. Protein lysates were resolved on SDS-PAGE in a 4-15% TRIS-glycine gel (BIO-RAD Mini -PROTEAN® TGX™) together with a molecular weight marker, Page Ruler Plus (ProteinTech). Gels were run for 1–2 h at 100 V until the ladder 10 kDa band was at the bottom of the gel. Nitrocellulose membrane 0.2-µM-pore-size (Amersham™ Protran®, GE Healthcare) was cut to size and wetted in transfer buffer. Wet transfer was completed in transfer buffer at 60 V for 45 min.

Membrane was blocked with 3% BSA TBST for 1 h, washed once in TBST and incubated overnight in primary antibody diluted in blocking buffer at 4 °C. The blot was washed 3x 5 min in TBST and incubated in a secondary antibody diluted 1:5000 in blocking buffer for 1 h. Blots were washed again 3x 5 min, TBST, developed using SuperSignal™ West Pico Plus Chemiluminescent Substrate (Thermo Scientific) and imaged on the gel imager (Azure, Q500).

IFA quantification analysis

IFA images were analysed by creating regions of interest (ROI) encompassing single parasites, or nuclei, in Image J. ROIs were created in ImageJ using the 'threshold, analyse particles' function. ROIs of between 500-5000 pixels were selected; overlapping cells and top-down cells were removed visually. For nuclei vs whole cell analyses, ROIs for the nuclei were made using DAPI channel images and then matched to whole cell ROIs using X, Y coordinates. Mean (average signal per cell), and Max (maximum signal pixel per cell) gray values were measured from each channel. One biological replicate was analysed for these analyses.

FIGURE LEGENDS

Figure 1: <u>*T. gondii* encodes homologues of cell cycle checkpoint kinases</u>

Proteins in the tree were selected from high percentage identity hits when human ATR, ATM, DNA-PK, mTOR, PI4K and PI3K were searched in protein BLAST against *T. gondii* GT1 (GCA_000149715.2). PIKKs from *S. cerevisiae* (GCA_000146045.2) and human, as well as PI3/4Ks from *Plasmodium knowlesi* (GCA_000006355.3), *Plasmodium berghei* (GCA_900002375.2) and *Plasmodium falciparum* (GCA_000002765.3) were also included. Node support values are bootstrap values as percentages of 1000 tree iterations. Branch lengths are expected substitutions per amino acid site, shown with scale bar. An expanded phylogenetic tree is shown in Figure S5: placement of *T. gondii* proteins is unaltered.

Figure 2: <u>Inducible knockdown of *Tg*ATM and *Tg*ATR</u>

A,B Constructs used for tagging the *Tg*ATM (A) and *Tg*ATR (B) genes in the *T. gondii* genome. DHFR*, dihydrofolate reductase (selectable marker gene).

C,D IFA showing HA-tagged *Tg*ATM (C) and *Tg*ATR (D) in intracellular tachyzoites: representative cells are shown from each tagged line, before and after addition of ATc for 24 h. Scale bar, 2 µm.

E,F Quantification of IFA signals in the parental control line (Δ*ku80*:TATi), each tagged line, and each knockdown (k/d, ATc treated for 24 h): *Tg*ATM (E) and *Tg*ATR (F). N = 50 parasites quantified per condition. Ordinary one-way ANOVA and post hoc Tukey's multiple comparisons tests of all samples; P values: *<0.05, **<0.01, ***<0.001, ****<0.0001. Comparisons not shown, ns.

Figure 3: Knockdown of *Tg*ATM or *Tg*ATR imposes no growth defect or sensitivity to DNA damage

A,B Images of three replicate plaque assays, either untreated (control) or treated with ATc to induce *Tg*ATM k/d (A) and *Tg*ATR k/d (B).

C,D Plaque assay images are shown with or without DNA damage, CPT or MMS, at the concentrations stated for 10 days. *Tg*ATM k/d (C) or *Tg*ATR k/d (D) parasites were pre-treated with ATc for 24 h and then additionally treated with DNA damaging agents for 10 days. Representative images from three biological replicates are shown.

Figure 4: Knockdown of *Tg*ATM or *Tg*ATR ablates acute checkpoint-like responses to DNA damage

A Images of representative vacuoles containing 2, 4, 8 or 16 parasites, as counted for the graphs in B and C after 24h growth. Scale bar 2 µm.

B,C Replication assays were conducted on *Tg*ATM k/d (A) and *Tg*ATR k/d (B) parasites, grown for 24h under DNA-damaging conditions. Numbers of parasites in 250 vacuoles were counted per condition in each experiment; data from 2-3 biological replicates are shown. Ordinary one-way ANOVA and post hoc Tukey's multiple comparisons tests were made of control vs all other conditions, and of each drug treatment vs k/d with the same treatment. P values: *<0.05, **<0.01, ***<0.001, ****<0.0001. Comparisons not shown, ns. Also not shown on the graph, for concision: the ATM control line differed from the same line under all DNA damage conditions at p-value ****<0.0001 , the ATR control also differed from all DNA damage conditions at p-value ****<0.0001 except ***<0.001 for 2.5uM CPT.

D,E IFA of H2AX phosphorylation in *Tg*ATM k/d (C) and *Tg*ATR k/d (D) tachyzoites that were treated for 2 h with DNA-damaging agents. Representative images from three biological replicates are shown. Scale bar 2 µm.

Figure 5: *Tg*ATR does not behave quantifiably differently in the presence or absence of *Tg*ATM

A Construct used to tag the *TgATR* gene with V5, under the tubulin (Tub) promoter and chloramphenicol resistance selectable marker (CAT). Also shown is the original construct used to tag the *TgATM* gene with HA.

B IFA showing parasites with both ATR and ATM tagged, as in A, in either control or *Tg*ATM knockdown conditions, treated with DNA damaging drug treatments for 2 h, 24 h after infection of fresh host cells. Scale bar, 2 µm.

C Using IFA images as in (B), maximum brightness of *Tg*ATR and *Tg*ATM foci was measured in both control and ATM-knockdown conditions, as well as in the parental line (Δ*ku80*:TATi). N = 50 parasites quantified per condition. One biological replicate was analysed in this experiment. Ordinary one-way ANOVA and post hoc Tukey's multiple comparisons tests of control vs all conditions for both *Tg*ATR and *Tg*ATM were completed; P values: *<0.05, **<0.01, ***<0.001, ****<0.0001. Comparisons not shown, ns.

D Mean brightness of *Tg*ATR and *Tg*ATM signals throughout parasites, measured in both control and ATM-knockdown conditions, as well as the parental line (Δ*ku80*:TATi). N = 50 parasites quantified per condition. Statistical analysis as in (C).

Figure 6: KU55933, an inhibitor of human ATM, does not phenocopy knockdown of *Tg*ATM or *Tg*ATR

A. Images of plaque assays conducted in the *Tg*ATM and *Tg*ATR HA-tagged lines treated with increasing concentrations of KU-55933.

B. Images of plaque assays showing the same lines as in (A), treated with KU-55933, after knockdown of *Tg*ATM or *Tg*ATR.

C. Using IFA images, the maximum brightness of *Tg*ATR and *Tg*ATM foci was measured in both control and ATM-knockdown conditions, with or without KU-55933. N = 50 parasites quantified per condition. One biological replicate was analysed in this experiment. Ordinary one-way ANOVA and post hoc Tukey's multiple comparisons tests of control vs all conditions for both *Tg*ATR and *Tg*ATM were completed; P values: *<0.05, **<0.01, ***<0.001, ****<0.0001. Comparisons not shown, ns.

D. Mean brightness of *Tg*ATR and *Tg*ATM signals throughout parasites, measured in both control and ATM-knockdown conditions, with or without KU55933. N = 50 parasites quantified per condition. Statistical analysis as in (C).

E. IFA showing parasites H2AX foci in control parasites treated or not treated with KU55933, with or without DNA-damaging drugs MMS or CPT. Scale bar, 2 µm.

SUPPLEMENTARY FIGURE LEGENDS

Figure S1: Inducible knockdown of *Tg*ATM and *Tg*ATR

A. The phenotype score for *Tg*ATM from a genome-wide CRISPR screen to identify essential genes in *T. gondii* (Sidik et al., 2016).

B. The phenotype score for *Tg*ATR from a genome-wide CRISPR screen to identify essential genes in *T. gondii* (Sidik et al., 2016).

C. The schematic shows where the primers were located for PCR-based testing of correct integration of the HA tag on the *ATM* gene. The PCR shows the correct size band was present in all ATM clones and not in the parental control line. Asterisks denote non-specific bands that amplified from both the parental line ('Δ*ku80*:TATi') and HA-tagged clones.

D. The schematic shows primers designed to test for correct integration of the HA tag on the *ATR* gene. The PCR shows correct integration in several clones and the absence of a product from the parental control line; an HA-tagged ATM control (as in C) is also shown.

E. Anti-HA western blot of samples from an ATM tagged clone, taken at 24, 48 and 72 h after the addition of ATc. Profilin was used as a control protein.

Figure S2: V5 tagging of *Tg*ATR in the HA-*Tg*ATM background

A. The schematics show where the primers were located for PCR-based testing of correct integration of the V5 tag on the *ATR* gene, and likewise for the original PCR-based testing of HA-tagging on the *ATM* gene (also shown in Fig S1).

B. The PCR result on the left shows the correct size band for V5-tagged *TgATR* after transfection of this construct into the *Tg*ATM-HA line. No band appeared in the parental control line ('Δ*ku80*:TATi') or in either single-gene-tagged line. The PCR on the right shows that the correct size band for HA-tagged *TgATM* remained in the double-tagged line.

Figure S3: The nuclear/cytoplasmic distribution of *Tg*ATR and *Tg*ATM does not change after DNA damage

Using IFA images as in Figure 5B, the amount of signal in the nucleus and in the whole cell was quantified for both *Tg*ATM (A) and *Tg*ATR (B), with or without ATM k/d and addition of 50µM CPT or 500µM MMS. N = 50 parasites per condition. One biological replicate was analysed in this experiment. Ordinary one-way ANOVA and post hoc Tukey's multiple comparisons tests of control vs all conditions for both *Tg*ATR and *Tg*ATM were completed; P values: *<0.05, **<0.01, ***<0.001, ****<0.0001. Comparisons not shown, ns.

Figure S4: ATc has no effect on the DNA damage checkpoint response of the host cell of *T. gondii*, whereas KU-55933 inhibits this response.

Immunofluorescence images showing that phosphorylation of H2AX in the host cell nucleus a) was not affected by addition of ATc, in cells either uninfected or infected with the parental line of *T. gondii*, Δ*ku80*:TATi; b) was inhibited upon addition of the KU-55933 inhibitor. Cells were treated with 0.5mg/ml ATc, 50 µM CPT, 50µM KU-55933, or combinations of these. Representative images from one biological replicate are shown. Scale bar 5 µm.

Figure S5: Apicomplexan parasites encode one, two, or no homologues of the cell cycle checkpoint kinases ATM and ATR

Proteins in the tree were selected from high percentage identity hits when human ATR, ATM, DNA-PK, mTOR, PI4K and PI3K were searched in protein BLAST against the genomes of *T. gondii* GT1 (GCA_000149715.2), *Theileria parva* (GCA_000165365.1), *Plasmodium knowlesi* (GCA_000006355.3), *Plasmodium berghei* (GCA_900002375.2), *Plasmodium gaboni* (GCA_001602025.1), *Plasmodium falciparum* (GCA_000002765.3), *Cystoisospora suis* (GCA_002600585.1), *Babesia microti* (GCA_000691945.2), *Cryptosporidium hominis* (GCA_002223825.1), *Schistosoma mansoni* (GCA_000237925.5), *Saccharomyces cerevisiae* (GCA_000146045.2), *Chromera velia* (GCA_900069035), *Leishmania major* (GCA_000002725.2), *Schizosaccharomyces pombe* (GCA_000002945.2), *Caenorhabditis elegans* GCA_000002985.6 and *Trypanosoma brucei* (GCA_000002445.2). The tree was rooted with the divergence of PI3K from PIKK sequences. Node support values are bootstrap values as percentages of 1000 tree iterations. Branch lengths are expected substitutions per amino acid site shown with scale bar.

Figure S6: Resource table

A. Table containing plasmid maps.

B. Table containing protospacer and primer sequences.

C. Table containing antibodies used.

FUNDING

This work was funded by the European Research Council (ERC) under the European Union's Horizon 2020 research and innovation programme (ERC-2016-COG 725126 to CJM); Wellcome Award 214298/Z/18/Z to RFW; and a PhD studentship from the University of Cambridge Department of Pathology to MJK.

REFERENCES

Absalon, S. and J. D. Dvorin (2021). "Depletion of the mini-chromosome maintenance complex binding protein allows the progression of cytokinesis despite abnormal karyokinesis during the asexual development of Plasmodium falciparum." Cell Microbiol **23**(3): e13284.
Alvarez, C. A. and E. S. Suvorova (2017). "Checkpoints of apicomplexan cell division identified in Toxoplasma gondii." PLoS Pathog **13**(7): e1006483.
Angel, S. O., L. Vanagas, D. M. Ruiz, C. Cristaldi, A. M. Saldarriaga Cartagena and W. J. Sullivan, Jr. (2020). "Emerging Therapeutic Targets Against Toxoplasma gondii: Update on DNA Repair Response Inhibitors and Genotoxic Drugs." Front Cell Infect Microbiol **10**: 289.
Araki, T., S. Kawai, S. Kakuta, H. Kobayashi, Y. Umeki, Y. Saito-Nakano, T. Sasaki, K. Nagamune, Y. Yasutomi, T. Nozaki, B. Franke-Fayard, S. M. Khan, H. Hisaeda and T. Annoura (2020). "Three-dimensional electron microscopy analysis reveals endopolygeny-like nuclear architecture segregation in Plasmodium oocyst development." Parasitol Int **76**: 102034.
Bakkenist, C. J. and M. B. Kastan (2003). "DNA damage activates ATM through intermolecular autophosphorylation and dimer dissociation." Nature **421**(6922): 499-506.
Barylyuk, K., L. Koreny, H. Ke, S. Butterworth, O. M. Crook, I. Lassadi, V. Gupta, E. Tromer, T. Mourier, T. J. Stevens, L. M. Breckels, A. Pain, K. S. Lilley and R. F. Waller (2020). "A Comprehensive Subcellular Atlas of the Toxoplasma Proteome via hyperLOPIT Provides Spatial Context for Protein Functions." Cell Host Microbe **28**(5): 752-766 e759.
Bogado, S. S., M. C. Dalmasso, A. Ganuza, K. Kim, W. J. Sullivan, Jr., S. O. Angel and L. Vanagas (2014). "Canonical histone H2Ba and H2A.X dimerize in an opposite genomic localization to H2A.Z/H2B.Z dimers in Toxoplasma gondii." Mol Biochem Parasitol **197**(1-2): 36-42.
Dalmasso, M. C., D. O. Onyango, A. Naguleswaran, W. J. Sullivan, Jr. and S. O. Angel (2009). "Toxoplasma H2A variants reveal novel insights into nucleosome composition and functions for this histone family." J Mol Biol **392**(1): 33-47.
Engler, C. and S. Marillonnet (2014). "Golden Gate cloning." Methods Mol Biol **1116**: 119-131.
Falck, J., J. H. Petrini, B. R. Williams, J. Lukas and J. Bartek (2002). "The DNA damage-dependent intra-S phase checkpoint is regulated by parallel pathways." Nat Genet **30**(3): 290-294.
Fenoy, I. M., S. S. Bogado, S. M. Contreras, V. Gottifredi and S. O. Angel (2016). "The Knowns Unknowns: Exploring the Homologous Recombination Repair Pathway in Toxoplasma gondii." Front Microbiol **7**: 627.
Francia, M. E. and B. Striepen (2014). "Cell division in apicomplexan parasites." Nat Rev Microbiol **12**(2): 125-136.
Gubbels, M. J., I. Coppens, K. Zarringhalam, M. T. Duraisingh and K. Engelberg (2021). "The Modular Circuitry of Apicomplexan Cell Division Plasticity." Front Cell Infect Microbiol **11**: 670049.
Gubbels, M. J., C. D. Keroack, S. Dangoudoubiyam, H. L. Worliczek, A. S. Paul, C. Bauwens, B. Elsworth, K. Engelberg, D. K. Howe, I. Coppens and M. T. Duraisingh (2020). "Fussing About Fission:

Defining Variety Among Mainstream and Exotic Apicomplexan Cell Division Modes." Front Cell Infect Microbiol **10**: 269.
Hawkins, L. M., A. V. Naumov, M. Batra, C. Wang, D. Chaput and E. S. Suvorova (2021). "Novel CRK-Cyclin Complex Controls Spindle Assembly Checkpoint in Toxoplasma Endodyogeny." mBio **13**(1): e0356121.
Heaslip, A. T., M. Nishi, B. Stein and K. Hu (2011). "The motility of a human parasite, Toxoplasma gondii, is regulated by a novel lysine methyltransferase." PLoS Pathog **7**(9): e1002201.
Helt, C. E., W. A. Cliby, P. C. Keng, R. A. Bambara and M. A. O'Reilly (2005). "Ataxia telangiectasia mutated (ATM) and ATM and Rad3-related protein exhibit selective target specificities in response to different forms of DNA damage." J Biol Chem **280**(2): 1186-1192.
Hutchison, W. M., J. F. Dunachie, J. C. Siim and K. Work (1970). "Coccidian-like nature of Toxoplasma gondii." Br Med J **1**(5689): 142-144.
Kalyaanamoorthy, S., B. Q. Minh, T. K. F. Wong, A. von Haeseler and L. S. Jermiin (2017). "ModelFinder: fast model selection for accurate phylogenetic estimates." Nat Methods **14**(6): 587-589.
Katris, N. J., G. G. van Dooren, P. J. McMillan, E. Hanssen, L. Tilley and R. F. Waller (2014). "The apical complex provides a regulated gateway for secretion of invasion factors in Toxoplasma." PLoS Pathog **10**(4): e1004074.
Keegan, K. S., D. A. Holtzman, A. W. Plug, E. R. Christenson, E. E. Brainerd, G. Flaggs, N. J. Bentley, E. M. Taylor, M. S. Meyn, S. B. Moss, A. M. Carr, T. Ashley and M. F. Hoekstra (1996). "The Atr and Atm protein kinases associate with different sites along meiotically pairing chromosomes." Genes Dev **10**(19): 2423-2437.
Matthews, H., C. W. Duffy and C. J. Merrick (2018). "Checks and balances? DNA replication and the cell cycle in Plasmodium." Parasit Vectors **11**(1): 216.
Matthews, H., J. McDonald, F. I. G. Totanes and C. J. Merrick (2022). "Dynamics of DNA replication during male gametogenesis in the malaria parasite Plasmodium falciparum." Cellular Microbiology.
Meissner, M., S. Brecht, H. Bujard and D. Soldati (2001). "Modulation of myosin A expression by a newly established tetracycline repressor-based inducible system in Toxoplasma gondii." Nucleic Acids Res **29**(22): E115.
Montazeri, M., S. Mehrzadi, M. Sharif, S. Sarvi, A. Tanzifi, S. A. Aghayan and A. Daryani (2018). "Drug Resistance in Toxoplasma gondii." Front Microbiol **9**: 2587.
Munera Lopez, J., A. Ganuza, S. S. Bogado, D. Munoz, D. M. Ruiz, W. J. Sullivan, Jr., L. Vanagas and S. O. Angel (2019). "Evaluation of ATM Kinase Inhibitor KU-55933 as Potential Anti-Toxoplasma gondii Agent." Front Cell Infect Microbiol **9**: 26.
Nardelli, S. C., F. Y. Che, N. C. Silmon de Monerri, H. Xiao, E. Nieves, C. Madrid-Aliste, S. O. Angel, W. J. Sullivan, Jr., R. H. Angeletti, K. Kim and L. M. Weiss (2013). "The histone code of Toxoplasma gondii comprises conserved and unique posttranslational modifications." mBio **4**(6): e00922-00913.
Neville, A. J., S. J. Zach, X. Wang, J. J. Larson, A. K. Judge, L. A. Davis, J. L. Vennerstrom and P. H. Davis (2015). "Clinically Available Medicines Demonstrating Anti-Toxoplasma Activity." Antimicrob Agents Chemother **59**(12): 7161-7169.
Perry, J. and N. Kleckner (2003). "The ATRs, ATMs, and TORs are giant HEAT repeat proteins." Cell **112**(2): 151-155.
Roos, D. S., R. G. Donald, N. S. Morrissette and A. L. Moulton (1994). "Molecular tools for genetic dissection of the protozoan parasite Toxoplasma gondii." Methods Cell Biol **45**: 27-63.
Sheiner, L., J. L. Demerly, N. Poulsen, W. L. Beatty, O. Lucas, M. S. Behnke, M. W. White and B. Striepen (2011). "A systematic screen to discover and analyze apicoplast proteins identifies a conserved and essential protein import factor." PLoS Pathog **7**(12): e1002392.
Sidik, S. M., D. Huet, S. M. Ganesan, M. H. Huynh, T. Wang, A. S. Nasamu, P. Thiru, J. P. J. Saeij, V. B. Carruthers, J. C. Niles and S. Lourido (2016). "A Genome-wide CRISPR Screen in Toxoplasma Identifies Essential Apicomplexan Genes." Cell **166**(6): 1423-1435 e1412.

Sinai, A. P. and E. S. Suvorova (2020). "The RESTRICTION checkpoint: a window of opportunity governing developmental transitions in Toxoplasma gondii." Curr Opin Microbiol **58**: 99-105.
Striepen, B., C. N. Jordan, S. Reiff and G. G. van Dooren (2007). "Building the perfect parasite: cell division in apicomplexa." PLoS Pathog **3**(6): e78.
Suvorova, E. S., M. Francia, B. Striepen and M. W. White (2015). "A novel bipartite centrosome coordinates the apicomplexan cell cycle." PLoS Biol **13**(3): e1002093.
Trifinopoulos, J., L. T. Nguyen, A. von Haeseler and B. Q. Minh (2016). "W-IQ-TREE: a fast online phylogenetic tool for maximum likelihood analysis." Nucleic Acids Res **44**(W1): W232-235.
Vonlaufen, N., A. Naguleswaran, I. Coppens and W. J. Sullivan, Jr. (2010). "MYST family lysine acetyltransferase facilitates ataxia telangiectasia mutated (ATM) kinase-mediated DNA damage response in Toxoplasma gondii." J Biol Chem **285**(15): 11154-11161.
Wu, Z. H., Y. Shi, R. S. Tibbetts and S. Miyamoto (2006). "Molecular linkage between the kinase ATM and NF-kappaB signaling in response to genotoxic stimuli." Science **311**(5764): 1141-1146.
Zhou, B. B. and S. J. Elledge (2000). "The DNA damage response: putting checkpoints in perspective." Nature **408**(6811): 433-439.

Figure 1:

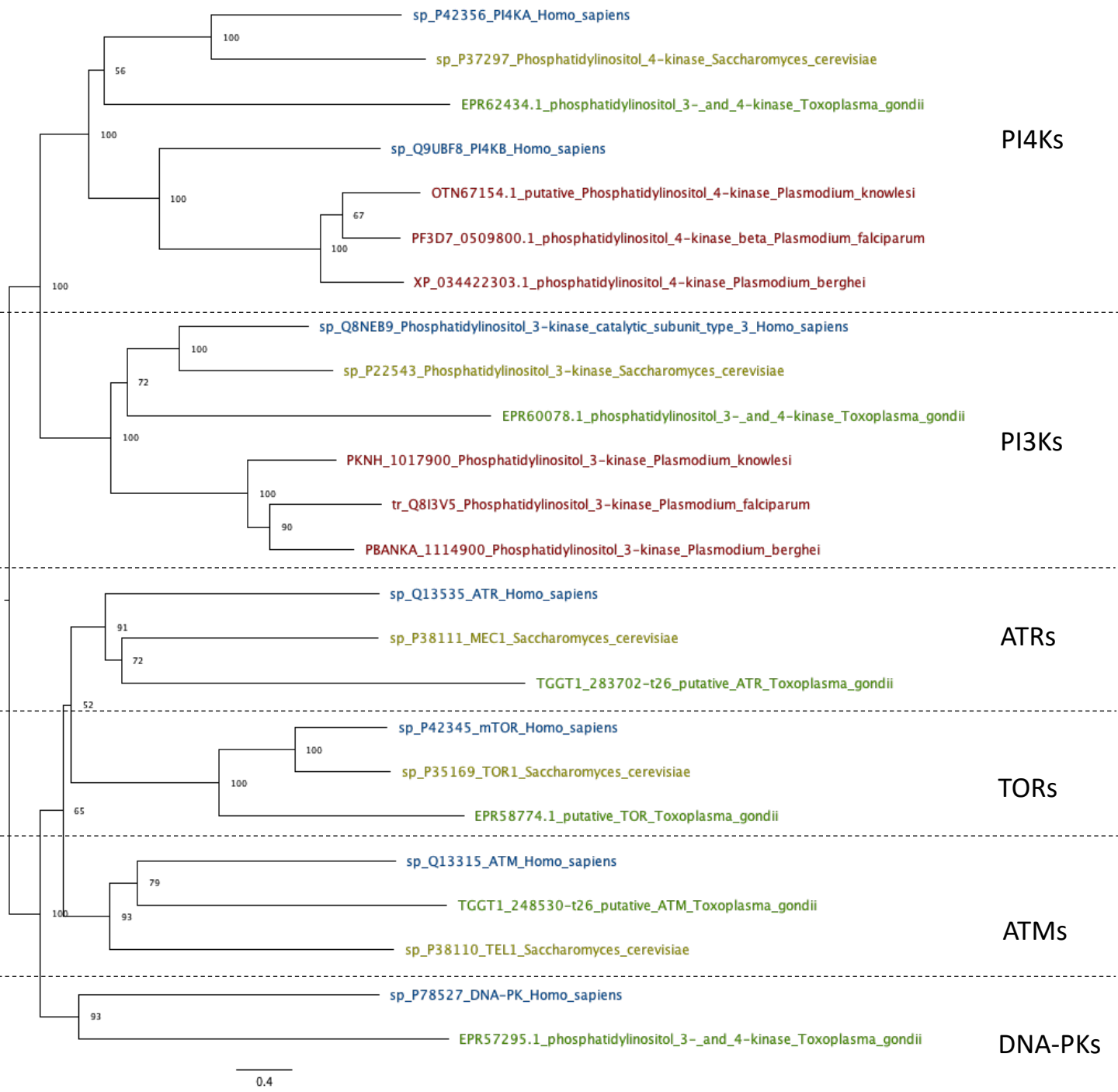
sp_P42356_PI4KA_Homo_sapiens
sp_P37297_Phosphatidylinositol_4-kinase_Saccharomyces_cerevisiae
EPR62434.1_phosphatidylinositol_3-_and_4-kinase_Toxoplasma_gondii
sp_Q9UBF8_PI4KB_Homo_sapiens
OTN67154.1_putative_Phosphatidylinositol_4-kinase_Plasmodium_knowlesi
PF3D7_0509800.1_phosphatidylinositol_4-kinase_beta_Plasmodium_falciparum
XP_034422303.1_phosphatidylinositol_4-kinase_Plasmodium_berghei
PI4Ks
sp_Q8NEB9_Phosphatidylinositol_3-kinase_catalytic_subunit_type_3_Homo_sapiens
sp_P22543_Phosphatidylinositol_3-kinase_Saccharomyces_cerevisiae
EPR60078.1_phosphatidylinositol_3-_and_4-kinase_Toxoplasma_gondii
PKNH_1017900_Phosphatidylinositol_3-kinase_Plasmodium_knowlesi
tr_Q8I3V5_Phosphatidylinositol_3-kinase_Plasmodium_falciparum
PBANKA_1114900_Phosphatidylinositol_3-kinase_Plasmodium_berghei
PI3Ks
sp_Q13535_ATR_Homo_sapiens
sp_P38111_MEC1_Saccharomyces_cerevisiae
TGGT1_283702-t26_putative_ATR_Toxoplasma_gondii
ATRs
sp_P42345_mTOR_Homo_sapiens
sp_P35169_TOR1_Saccharomyces_cerevisiae
EPR58774.1_putative_TOR_Toxoplasma_gondii
TORs
sp_Q13315_ATM_Homo_sapiens
TGGT1_248530-t26_putative_ATM_Toxoplasma_gondii
sp_P38110_TEL1_Saccharomyces_cerevisiae
ATMs
sp_P78527_DNA-PK_Homo_sapiens
EPR57295.1_phosphatidylinositol_3-_and_4-kinase_Toxoplasma_gondii
DNA-PKs
0.4

Figure 2:

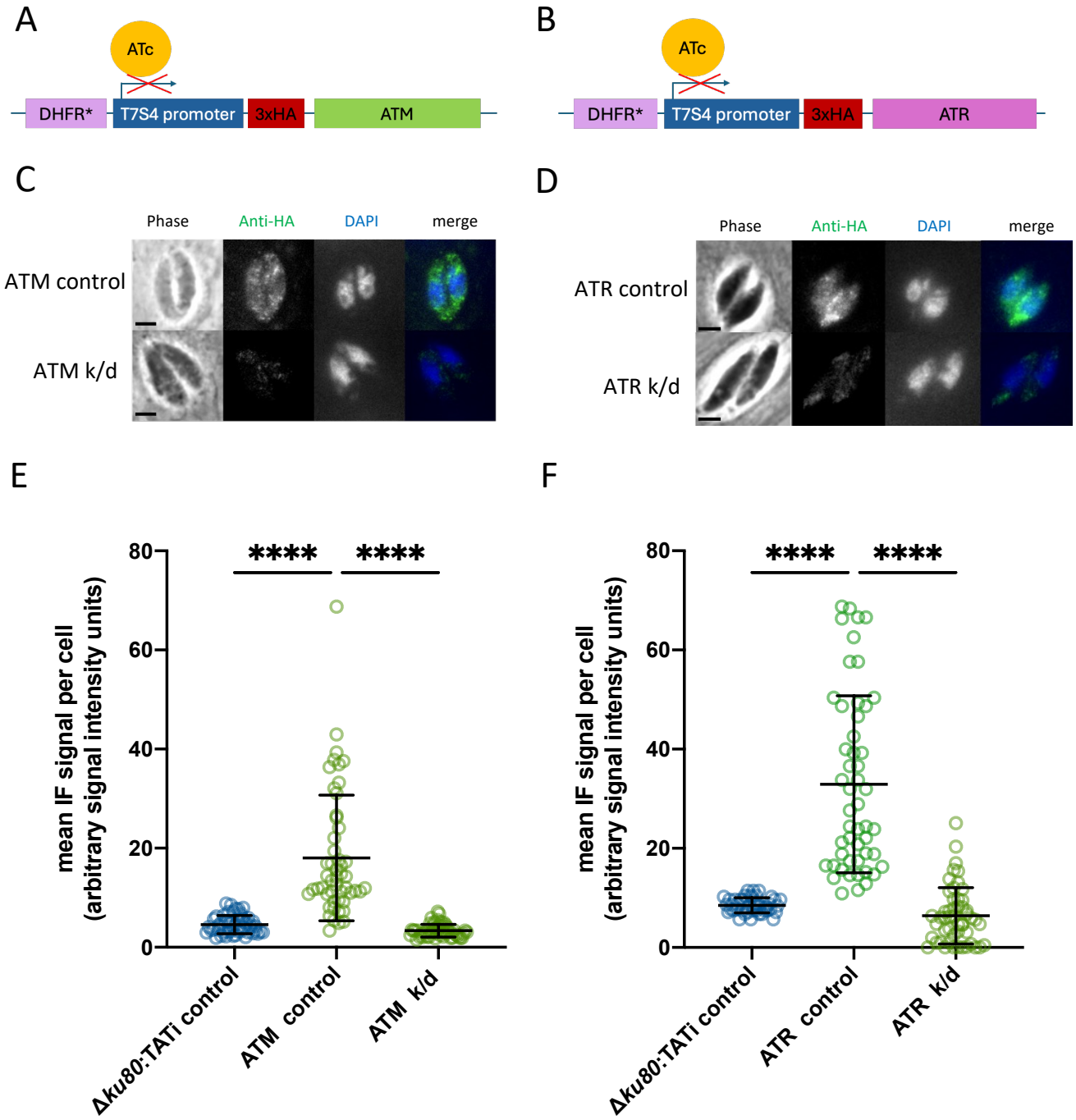
A
ATc
DHFR*
T7S4 promoter
3xHA
ATM
B
ATc
DHFR*
T7S4 promoter
3xHA
ATR
C
Phase
Anti-HA
DAPI
merge
ATM control
ATM k/d
D
Phase
Anti-HA
DAPI
merge
ATR control
ATR k/d
E
mean IF signal per cell
(arbitrary signal intensity units)
80
60
40
20
0
****
****
Δku80:TATi control
ATM control
ATM k/d
F
mean IF signal per cell
(arbitrary signal intensity units)
80
60
40
20
0
****
****
Δku80:TATi control
ATR control
ATR k/d

Figure 3:

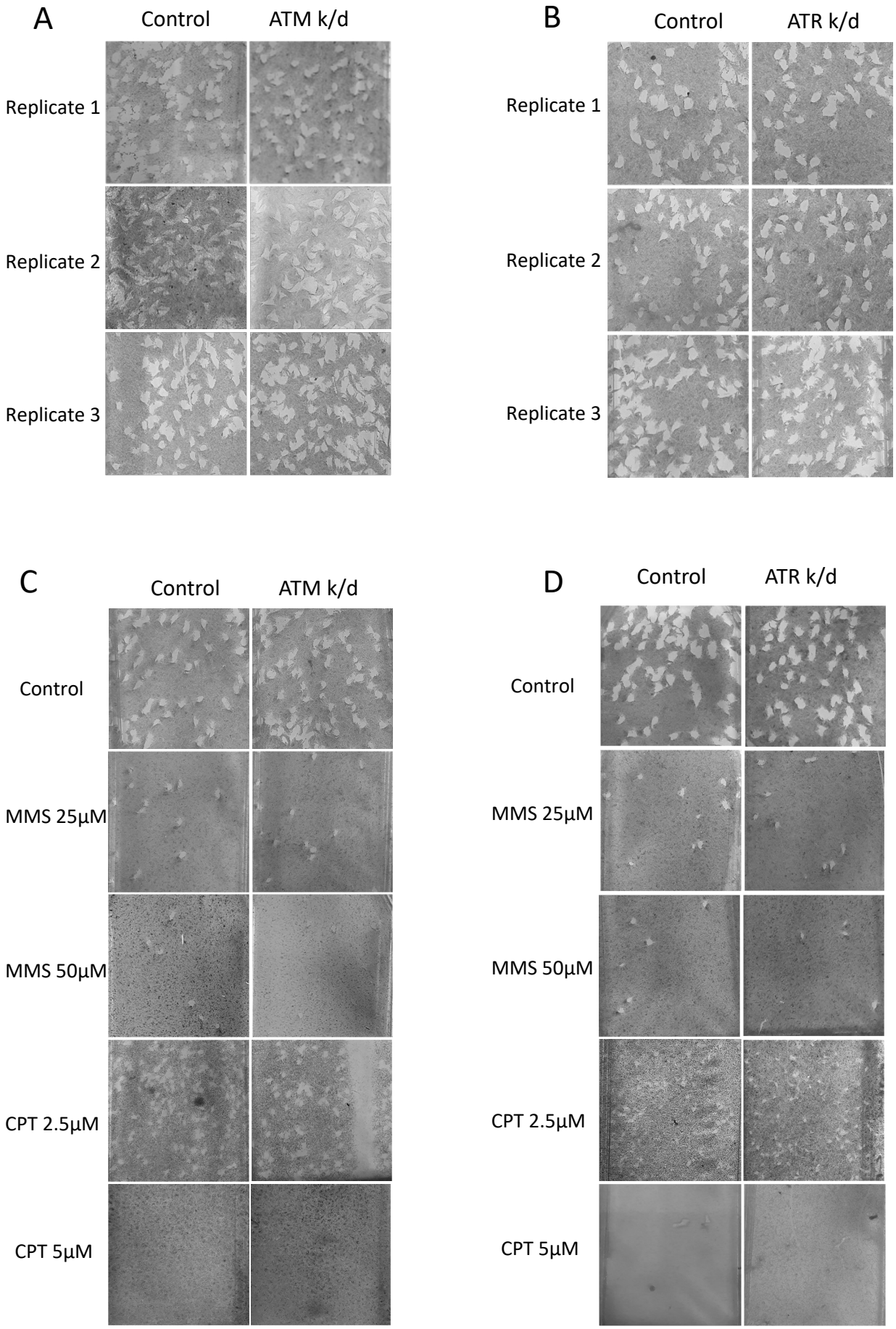
A
Control
ATM k/d
Replicate 1
Replicate 2
Replicate 3
B
Control
ATR k/d
Replicate 1
Replicate 2
Replicate 3
C
Control
ATM k/d
Control
MMS 25µM
MMS 50µM
CPT 2.5µM
CPT 5µM
D
Control
ATR k/d
Control
MMS 25µM
MMS 50µM
CPT 2.5µM
CPT 5µM

Figure 4:

A

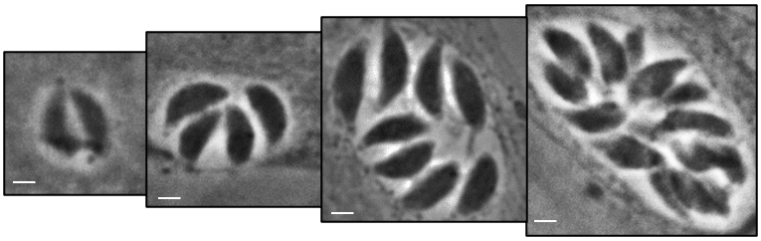

B

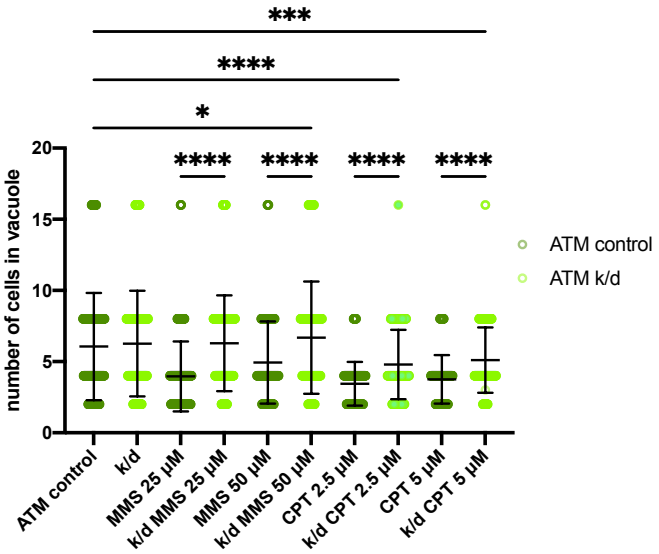

C

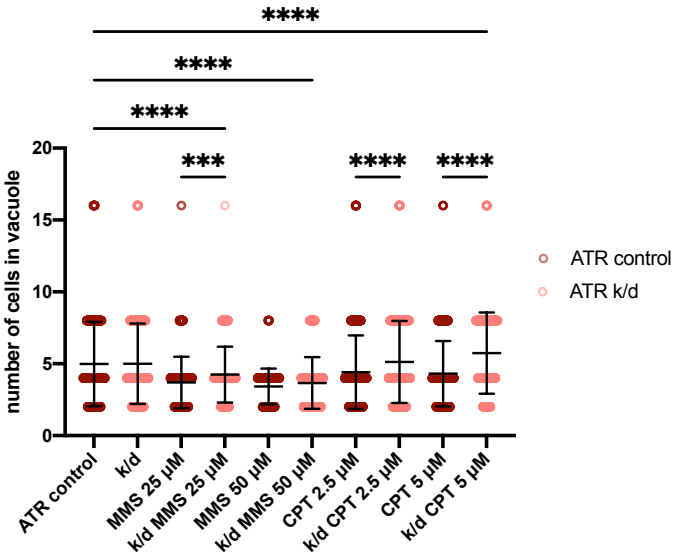

D

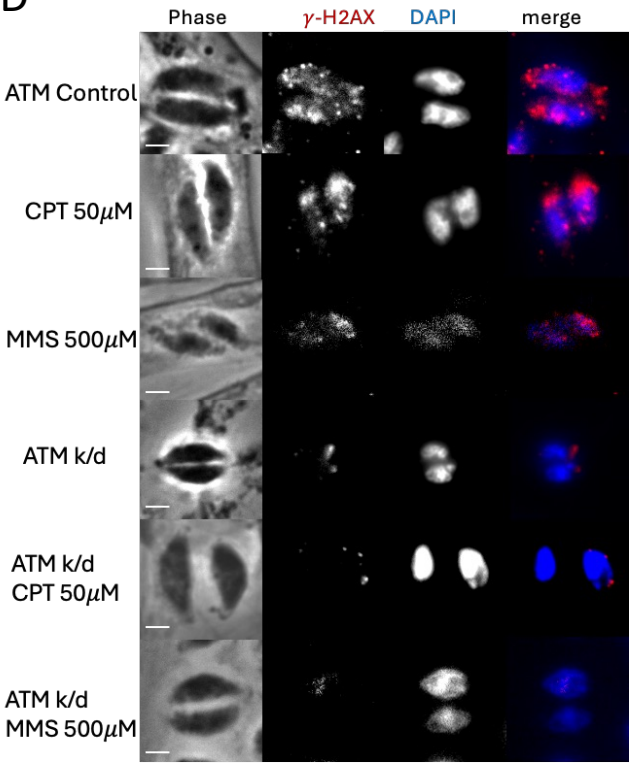

E

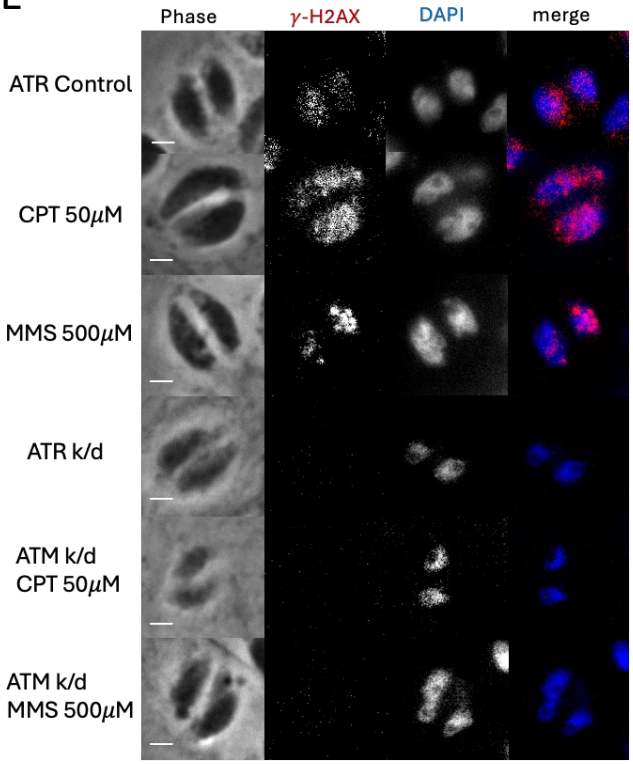

Figure 5:

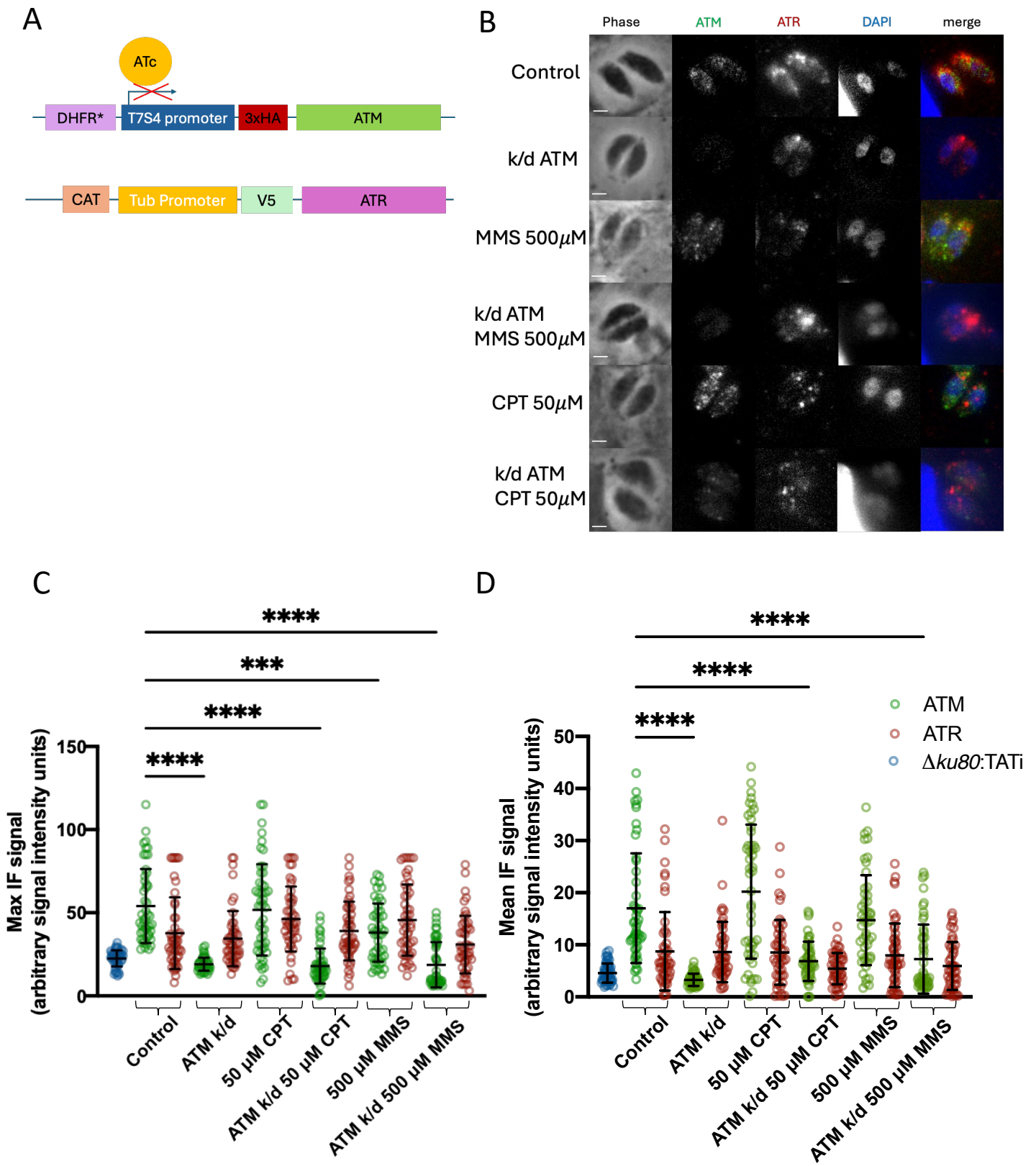
A
ATc
DHFR*
T7S4 promoter
3xHA
ATM
CAT
Tub Promoter
V5
ATR
B
Phase
ATM
ATR
DAPI
merge
Control
k/d ATM
MMS 500μM
k/d ATM
MMS 500μM
CPT 50μM
k/d ATM
CPT 50μM
C
Max IF signal
(arbitrary signal intensity units)
150
100
50
0
****
***
****
****
Control
ATM k/d
50 μM CPT
ATM k/d 50 μM CPT
500 μM MMS
ATM k/d 500 μM MMS
D
Mean IF signal
(arbitrary signal intensity units)
50
40
30
20
10
0
****
****
****
ATM
ATR
Δku80:TATi
Control
ATM k/d
50 μM CPT
ATM k/d 50 μM CPT
500 μM MMS
ATM k/d 500 μM MMS

Figure 6:

A

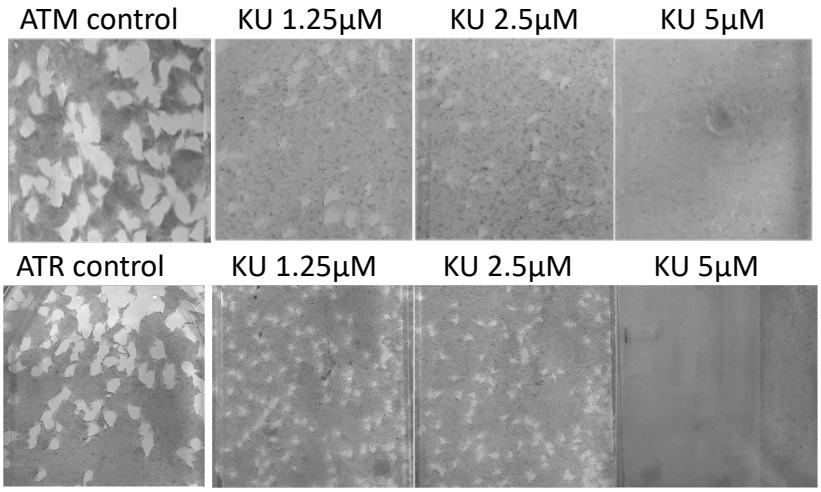

B

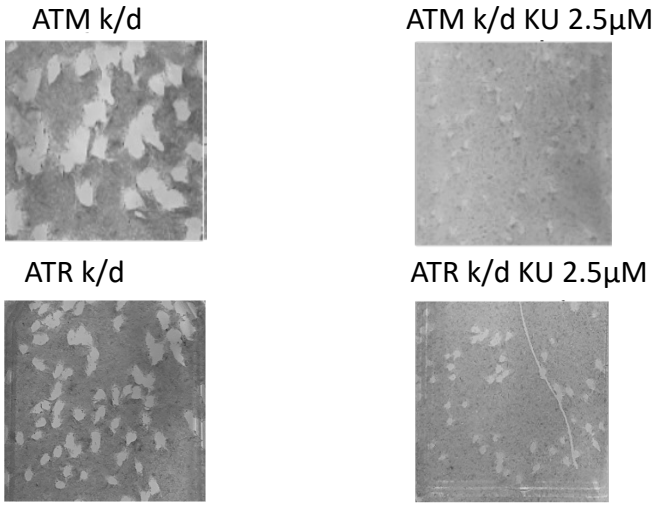

C

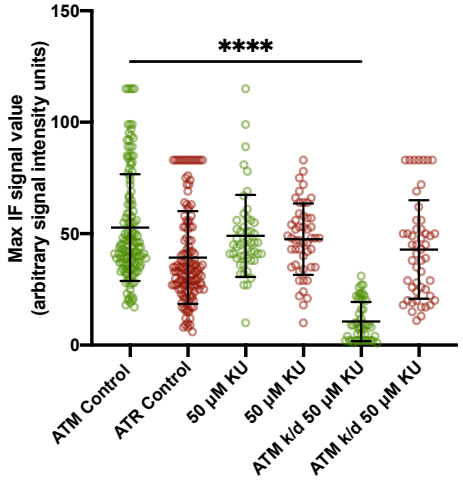

D

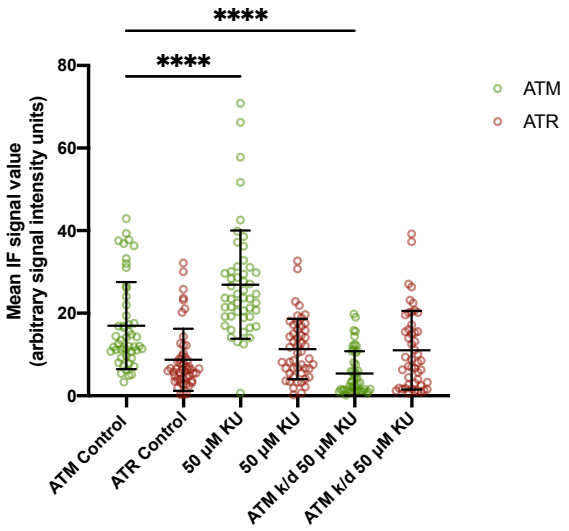
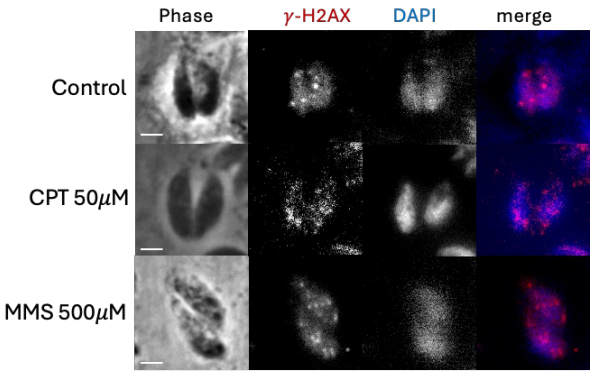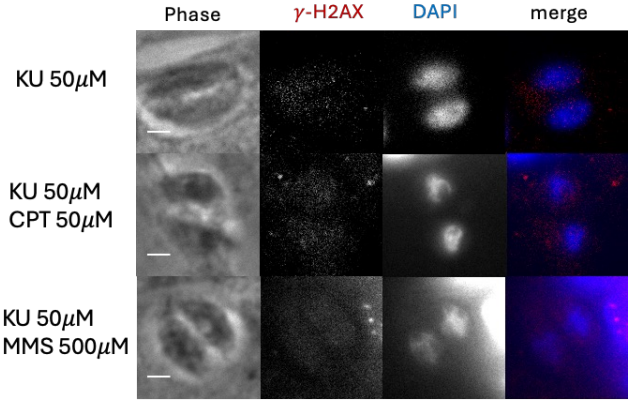
E